Journal of Solid State Chemistry **161,** 385–395 (2001)
doi:10.1006/jssc.2001.9352, available online at http://www.idealibrary.com on IDEAL®

Microdomains and Diffuse Scattering in $K_2In_{12}Se_{19}$

L. Kienle[1] and A. Simon

Max Planck Institut für Festkörperforschung, Heisenbergstrasse 1, 70569 Stuttgart, Germany

Received May 1, 2001; in revised form July 30, 2001; accepted August 9, 2001

Electron and X-ray diffraction studies on the new compound $K_2In_{12}Se_{19}$ indicate disorder of one-dimensional units due to the existence of pronounced diffuse scattering. The diffuse intensities are torus-shaped, with the axes of the rings collinear to c^*. Observations by high-resolution electron microscopy (HREM) confirm the presence of three-dimensionally ordered domains with variable size which are separated by antiphase boundaries. The sizes of the domains determine the shape of the diffuse intensity. Starting from the average structure it is possible to develop a model of domains which are three-dimensionally ordered. This model serves as a basis for simulated HREM images and electron diffraction patterns that show good agreement with experimental data. The diffuse scattering could be simulated qualitatively on the basis of a nonperiodic model of the real structure which consists of randomly packed rods. © 2001 Academic Press

Key Words: **electron diffraction; high-resolution electron microscopy; diffuse scattering; antiphase boundaries; real structure; simulation.**

INTRODUCTION

Many mixed-valence indium chalcogenides contain identical blocks of structural elements which could be regarded as "bricks" (1) establishing different crystal structures and chemical compositions through variable combinations of their connection. Like with a construction kit, it should be possible to predict the structure and composition of hypothetical compounds. The initial motivation for preparations in the system K–In–Se was the search for new ternary mixed-valence selenides of potassium and indium consistent with the predictions derived from the construction kit.

A by-product of these syntheses was red crystals of the normal valence compound $K_2In_{12}Se_{19}$, which crystallizes in a new structure type according to X-ray diffraction analysis on single crystals. They showed a combination of sharp Bragg reflections and ring-shaped diffuse intensities indicating a deviation from a strictly three-dimensionally ordered structure (2, 3). Temperature-dependent X-ray diffraction (4) on single crystals shows a significant decrease in intensity of the diffuse scattering with increasing temperature. The observations could be interpreted in terms of two distinguishable types of disorder, a static one at low temperatures and a dynamic one at higher temperatures. At 670 K a high-temperature phase of $K_2In_{12}Se_{19}$ is formed and the diffuse scattering completely disappears. The distribution of diffuse intensity could easily be visualized by inspection of reciprocal layers perpendicular to c^*. Every second layer in this direction exhibits only diffuse rings.

Circular features of diffuse scattering have been reported frequently in recent years, e.g., for quasicrystals (5) and many compounds related to the fluorite-type structure ((6) and references quoted therein) including the important oxygen ion conductors CSZ (7) and YSZ (8). In the case of the fluorite phases several experimental methods and simulation procedures were used; however, no unifying model of the real structure could be established despite very similar diffuse features for many compounds with different compositions. A common starting point for the description of the real structure of these compounds is based on static perturbations of the fluorite structure by the formation of small regions with an ordered structure (9, 10). The nature of the ordered regions could not be elucidated, and several models were established on the basis of clusters (11) or domains with a three-dimensionally ordered structure, which are for instance separated by antiphase boundaries (APBs) (8). These great variations in the structure models emphasize the problems of the interpretation of diffuse scattering in general. A prerequisite to analyze diffuse scattering is the solution of the average structure ($T_{measure}$ = 293 K) omitting all diffuse scattering and refining the structure on the basis of the Bragg reflections by conventional X-ray methods. For $K_2In_{12}Se_{19}$ this strategy led to a new structure type (space group $R\bar{3}$, $a = 13.852(2)$ Å, $c = 17.595(4)$ Å) including statistical disorder. The disorder is limited to 50% of all indium atoms which partially occupy centers of face-sharing Se_4 tetrahedra (positions In2 and In3). The site occupation factors (sof) of these indium atoms converge to approximately 0.5. Due to the connection of the tetrahedra the interatomic distances of the

[1]To whom correspondence should be addressed. Fax: +49-07116891091. E-mail: lkienle@sim.mpi-stuttgart.mpg.de.

0022-4596/01 $35.00

disordered indium atoms are unreasonably short ($d_{In-In} = 1.149$ Å), and it is quite obvious that the average structure has no physical meaning with respect to the indium sites. Apart from this discrepancy the structure refinement does not exhibit any crystallographic anomalies, like pronounced anisotropic thermal displacements or the necessity to include split positions. These observations are first indications that the relationship between the average and the real structure must be well defined.

The main goal of our investigations by electron microscopy was to work out the nature of the statical disorder by interpretation of the diffuse scattering phenomena and to develop reasonable models of the real structure of $K_2In_{12}Se_{19}$ on the basis of experimental data.

EXPERIMENTAL

$K_2In_{12}Se_{19}$ could be prepared (12) by heating (1270 K for 3 h) stoichiometric mixtures of the elements in evacuated dry quartz glass ampoules. Annealing at 950 K for 14 days leads to a homogeneous sample and the formation of well-shaped crystals. Selected single crystals of $K_2In_{12}Se_{19}$ were crushed in an agate mortar under *n*-butanol to obtain thin wedge-shaped crystallites. A perforated carbon/copper net was coated with the suspension, leaving the crystallites in random orientations after drying. These nets were fixed in a side-entry, double-tilt holder with the tilting limited to a maximum of $\pm 25^\circ$ in two directions. The electron microscopy studies were performed with a Philips CM30/ST (spherical aberration constant $C_S = 1.15$ mm) equipped with a LaB_6 cathode. Operating at a voltage of 300 kV the point resolution is 1.9 Å. SAED patterns were obtained using a diaphragm which limited the diffraction to a selected area of 2500 Å in diameter. Computer simulations of kinematical electron diffraction patterns and HREM images (multislice formalism) were performed using the EMS program package (13) (parameters for the image simulation: defocus spread $\Delta = 70$ Å, illumination semiangle $\alpha = 1.2$ mrad). Fourier transforms of high-resolution images were calculated using the software Digital Micrograph 2.5 (Gatan). HREM images and SAED patterns were recorded with a Slow Scan CCD Camera (Gatan, 1024×1024 pixels). In order to reduce noise all HREM images were filtered after Fourier transformation using a band-pass mask, with no loss of essential structural information in the following Fourier transformation.

RESULTS

SAED

First we examined several diffraction patterns obtained by tilting experiments in order to analyze shape and systematic appearance of diffuse intensities. All zone axis patterns exhibit sharp Bragg reflections that can be indexed assuming the cell has disordered average structure. In most of the observed diffraction patterns additional diffuse intensities appear on well-defined positions between the Bragg reflections. Except for the presence of diffuse intensities there is no indication of a symmetry reduction of the average structure. In order to describe the positions of the diffuse intensities a double cell ($a_{double} = a_{average}$, $c_{double} = 2c_{average}$) is used and indexing and all directions refer to the new cell. Diffuse scattering is limited to layers in reciprocal space perpendicular to c^* and occur only at the positions *hkl* with $l = 2n + 1$. The diffuse intensities symmetrically surround those positions with no observed Bragg reflections. For instance the SAED patterns of the zone axes [001], [241], and [$\bar{4}$41] show diffuse scattering not in the zero-order Laue zone (ZOLZ) but in the first-order Laue zone (FOLZ), as observed via convergent beam diffraction (CBED, microdiffraction (14, 15)). The shape of the diffuse scattering manifests itself in many examined ZOLZ as two sharp and very close intensity maxima separated by approximately 0.02 $Å^{-1}$. The pairs of maxima result from cutting the torus-shaped diffuse intensities through their centers. The orientation of these two maxima depends on the respective zone axis and can be predicted using stereographic projections of real and reciprocal space. We found that the vector within the reciprocal layer which is orthogonal to the connection line between two intensity maxima together with the adjusted zone axis and c^* are located on the same great circle. For instance in the diffraction patterns of the zone axes orientations [100], [$\bar{1}$11], and [122] (see Fig. 1) the connection lines are perpendicular to [001]*, [$\bar{1}\bar{1}$2]*, and [01$\bar{1}$]*. For several crystallites [01$\bar{1}$]* could be orientated perpendicular to the beam direction, and e.g. the zone axes patterns [511] and [$\bar{4}$11] could be obtained. Consistent with the stereographic projections these patterns are characterized by diffuse intensity doubles slightly tilted from parallel orientation to [01$\bar{1}$]*. By the combination of different sections through reciprocal space we conclude that the three-dimensional diffuse intensities could be characterized as torus-shaped; the axes of the rings are parallel to c^*.

According to the dynamical disorder (see temperature-dependent X-ray analysis in (4)) we expected crystals cooled with variable speed to show differences in the intensities of the diffuse scattering. Surprisingly, such differences were not detected for crystals quenched from 700 K to liquid nitrogen temperatures and crystals cooled at 10 K/min, respectively. Only upon close examination we observed slight variations for the distance between the diffuse intensity maxima in SAED.

As a first conclusion, because there is no streaking of all Bragg and diffuse intensities along c^*, the crystallites are well ordered in one direction ([001]) only. During the SAED observations we also found ordered crystallites without any occurrence of diffuse scattering. Those crystallites exhibit sharp reflections exactly located at the positions *hkl*

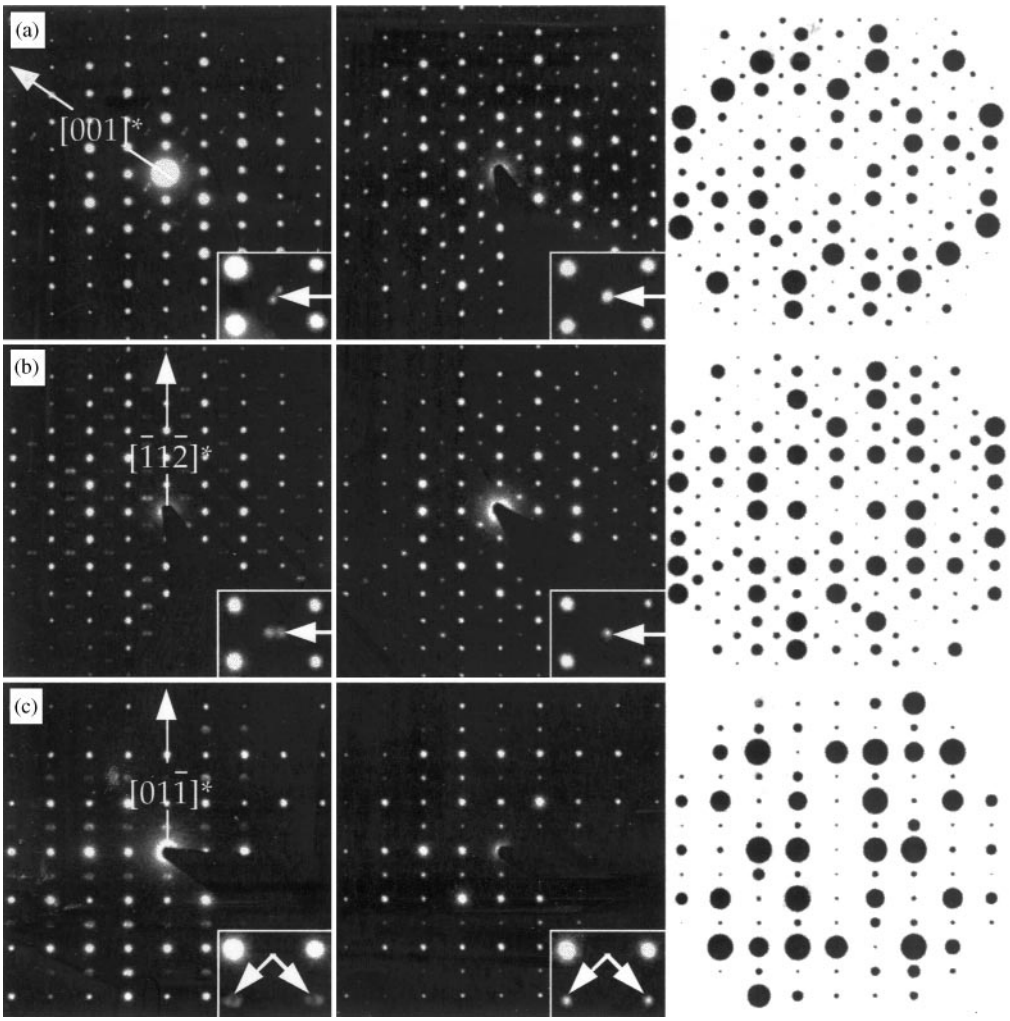

FIG. 1. SAED on static disordered (left) and ordered (middle) crystallites of $K_2In_{12}Se_{19}$ for zone axes [100] (a), [$\bar{1}$11] (b), and [122] (c). Enlarged sections are inserted showing examples for diffuse and superstructure reflections (see arrows). The reciprocal directions perpendicular to the orientations of the double spots with diffuse intensity are marked in the diffraction patterns of the statically disordered crystals (left). Right: simulations of the diffraction patterns (kinematical approximation) of the ordered crystals using the data of model A or B, see Table 1.

with $l = 2n + 1$; see for instance the diffraction patterns in Fig. 1 (zone axes patterns of [100], [$\bar{1}$11], and [122]). All reflections could be indexed on the basis of the doubled cell (see above), the Laue class is $\bar{3}$. By analyzing the reflection conditions we concluded that only two spacegroups are meaningful to describe the structure of the ordered crystals: $R3$ and $R\bar{3}$.

Three-Dimensionally Ordered Structures

The main purpose of this section is to develop reasonable structure models for the ordered crystals of $K_2In_{12}Se_{19}$ starting without any restrictions from symmetry. Taking into account the experimentally observed doubling of the c-axis (referring to the hexagonal setting) the average structure was transformed to space group $P1$ with the metrics of a rhombohedral cell, $a = b = c = 14.193$ Å, $\alpha = \beta = \gamma = 58.43°$.

By full occupation of 12 (from 24 possible) positions of the indium atoms we derived 2,704,156 different ordered structure models. The number of meaningful superstructures could be decreased by considering four essential structural requirements: (I) the meaningless short interatomic distances ($d_{In-In} = 1.149$ Å) between disordered indium positions in the average structure must be avoided. (II) At least one position derived from In2 in the average structure must be occupied, because the coordination sphere of the atom Se1 consists of six positions In2 exclusively. These two requirements decrease the number of possible ordered structures to 4095. Taking into account that the average structure is an artifact generated by some kind of superposition, the number of possible ordered structures could be decreased

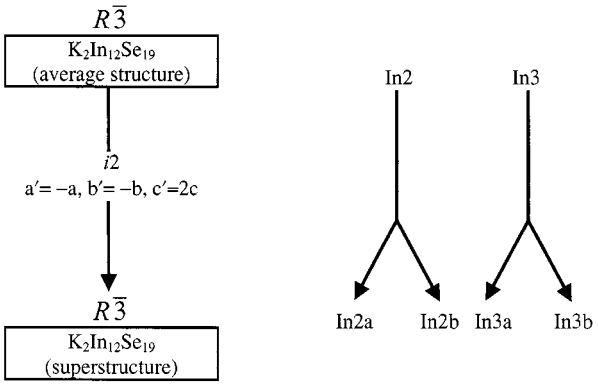

FIG. 2. Left: Group–subgroup relationship between the average structure and the superstructure of $K_2In_{12}Se_{19}$. Right: Splitting of In2 and In3.

further. The positions In2 and In3 of the average structure are occupied with equal weight (sof = 0.5) which cannot result from any superposition of In2 and In3. Hence there is the requirement (III) that, from all transformed positions of In2 and In3, six must be occupied, leading to 924 possible ordered structures. Excluding distances below $d_{In-In} =$ 3.39 Å as requirement (IV) results in four possible ordered structures that can be regarded as two pairs of related structures. These are characterized by higher symmetries than $P1$.

Two of them are enantiomorphs and can be described in the space group $R3$ without any need of doubling the c-axis of the trigonal single cell of the average structure. The observed superstructure reflections exclude these structure models.

The second pair of structures (in the following called model A and model B) must be described with the doubled cell in space group $R\bar{3}$. Using the crystallographic group–subgroup relation (16, 17, see Fig. 2), the symmetry reduction of the average structure is consistent with an isomorphous transition ($i2$). This transition is characterized by a doubling of the cell ($c_{double} = 2c_{average}$) and a splitting of each position of indium atoms, for instance the positions In2 and In3 of the disordered structure model into In2a,b and In3a,b. An alternating and full occupation of two of the four available positions was introduced as the basis for the ordering of the indium atoms and the formation of the superstructure. In the case of model A the positions In2a and In3b are occupied; model B is characterized by a full occupation of the positions In2b and In3a. It is important to note that these two structures are related by a vectorial shift of $\frac{1}{2}\vec{c}$ (see Table 1). Both exhibit the same diffraction pattern.

The shift could be regarded as a pseudotranslation conserved from the higher symmetry of the average structure. In fact all atoms are reproduced by this pseudotranslation

TABLE 1
Atomic Coordinates for the Superstructure Models A and B; Occupied Positions Are Marked

Atom	Site	x	y	z	Model A	Model B
K1a	6c	$\frac{1}{3}$	$\frac{2}{3}$	0.08340	×	×
K1b	6c	$\frac{1}{3}$	$\frac{2}{3}$	0.58340	×	×
Se1	6c	$\frac{2}{3}$	$\frac{1}{3}$	0.08333	×	×
Se2a	18f	0.14811	0.73188	0.62154	×	×
Se2b	18f	0.14811	0.73188	0.12154	×	×
Se3a	18f	0.47638	0.29736	0.67899	×	×
Se3b	18f	0.47638	0.29736	0.17899	×	×
Se4a	18f	0.43155	0.01447	0.60151	×	×
Se4b	18f	0.43155	0.01447	0.10151	×	×
In1a	18f	0.53954	0.98232	0.65838	×	×
In1b	18f	0.53954	0.98232	0.15838	×	×
In2a	18f	0.78274	0.25364	0.11779	×	
In2b	18f	0.78274	0.25364	0.61779		×
In3a	18f	0.55533	0.04380	0.54601		×
In3b	18f	0.55533	0.04380	0.04601	×	

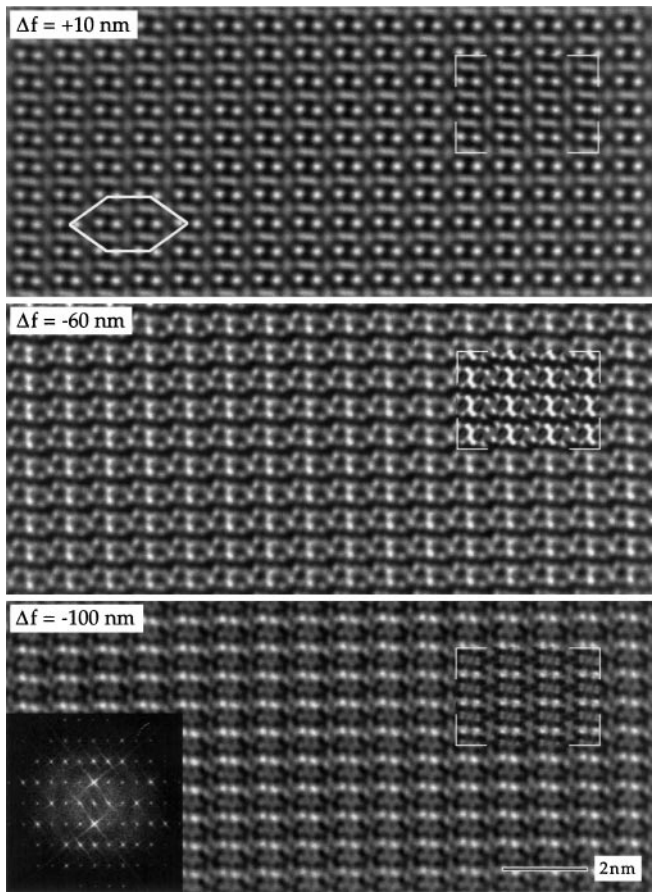

FIG. 3. High-resolution images of a disordered region (case (I), see text) in the orientation [$\bar{1}11$] with different defocus values (Δf); computer-simulated images are shown as insets (thickness $t = 84$ Å). The unit cell in this projection is displayed in the image with $\Delta f = 100$ Å; the FFT was calculated from a square section of an image with $\Delta f = -1000$ Å.

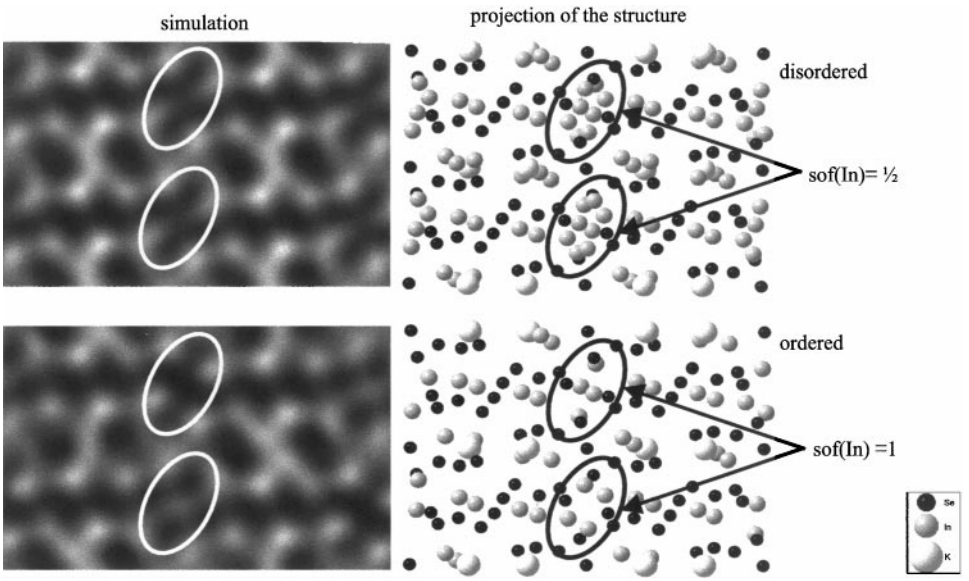

FIG. 4. Structural interpretation of the high-resolution images (orientation [$\bar{1}11$]) for disordered and ordered regions of the crystals. The simulated images were calculated at Scherzer defocus ($t = 28$ Å).

except for the indium atoms which cause the superstructure and which are found to be disordered in the model of the average structure. These superstructure models allow us to calculate the positions and intensities of all reflections for the structure of the ordered crystal. The simulated patterns (see Fig. 1) are in convincing agreement with the observed ones.

HREM

Several orientations of the crystallites were examined by HREM, for instance those with prominent diffuse scattering in the electron diffraction patterns. For all orientations except zone axes [001], [241], and [$\bar{4}41$] regions of the crystallites could be examined which are characterized by disorder resulting in diffuse intensities in Fourier transforms of these images.

It is useful to separate the ordering phenomena of the observed crystallites into three categories (I)–(III) according to the contrast of the images and the shape and the existence of intensities at positions hkl with $l = 2n + 1$ in the fast Fourier transforms (FFTs) of the images.

(I) Disordered regions of the crystallites without any indication of short range order show good agreement with simulated images calculated on the basis of the average structure model; see the series of images in Fig. 3 (zone axis [$\bar{1}11$]). The disorder leads to images with no periodic differences in contrast at different defocus values that could be associated with the doubling of the unit cell due to the ordering of the indium atoms. The structural interpretation of the contrasts in Fig. 4 by a comparison of the simulated image with the projection of the average structure clearly indicates that the disorder of the indium atoms results in

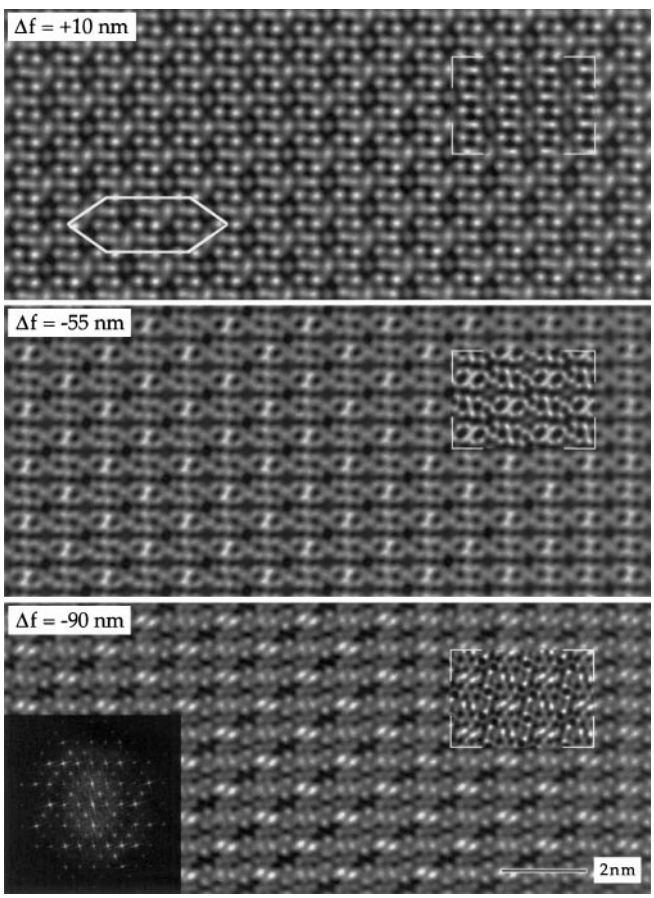

FIG. 5. High-resolution images of an ordered region (case (II)) in the orientation [$\bar{1}11$] with different defocus values (Δf); computer-simulated images are shown as insets ($t = 84$ Å). The unit cell in this projection is displayed in the image with $\Delta f = 100$ Å; the FFT was calculated from a square section of an image with $\Delta f = -900$ Å.

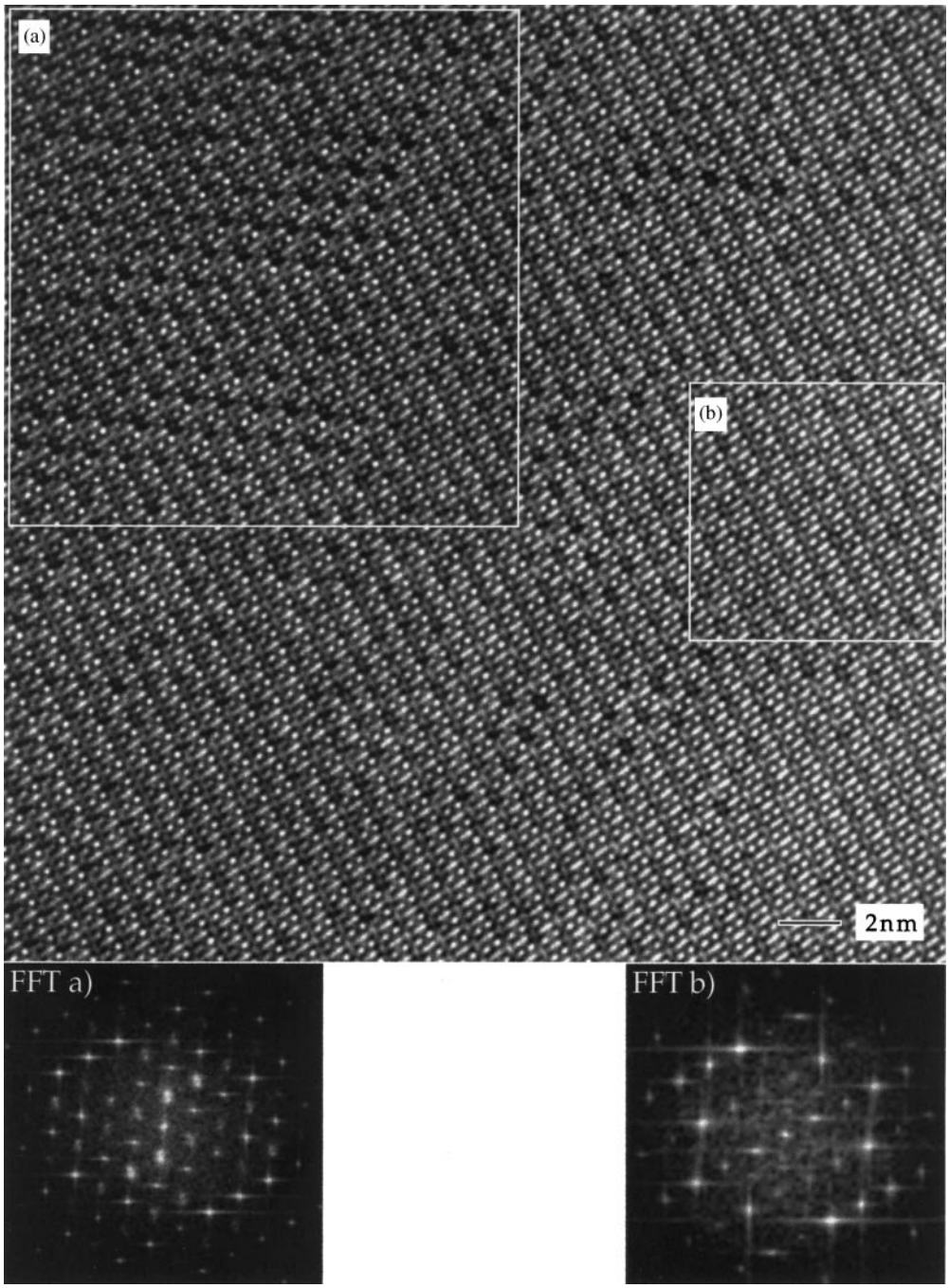

FIG. 6. Crystallite with ordered microdomains (case (III)). HREM image ($\Delta f = 100$ Å) in the orientation [$\bar{1}11$] with Fourier transforms of selected regions (a) and (b) showing strong differences in the intensity of the diffuse scattering.

identical contrast in the marked regions of the simulated image. The FFTs of the experimental images exhibit neither reflections *hkl* with $l = 2n + 1$ nor diffuse intensities in the surrounding of these positions, see Fig. 3, but only the Bragg intensities consistent with the disordered average structure. It should be mentioned that SAED patterns of such crystals always indicate weak additional intensities (sharp or diffuse) at or near the positions *hkl* with $l = 2n + 1$ confirming that the disordered regions without any significant short-range order of the crystallites are very small.

(II) Three-dimensionally ordered crystallites with long-range order and sharp superstructure reflections *hkl*, $l = 2n + 1$, in the FFTs of the images are shown in Fig. 5. In contrast to the observations on the crystallites of case (I)

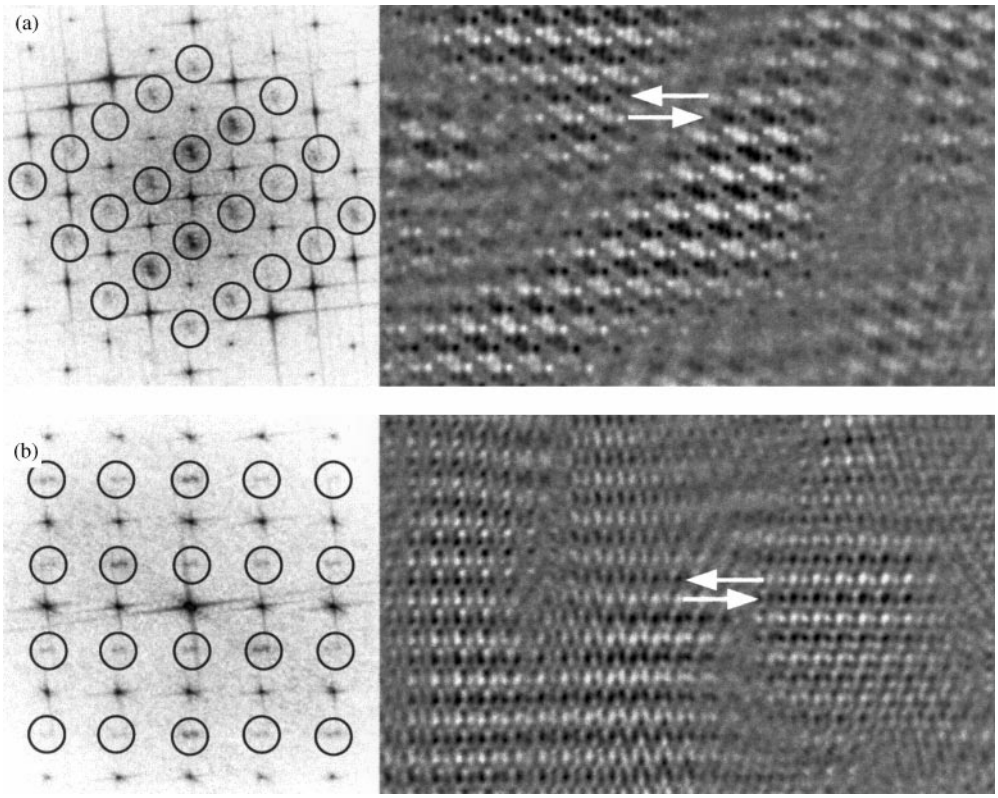

FIG. 7. Visualization of APDs. Inverse Fourier transforms of images in the orientations (a) $[\bar{1}11]$ and (b) [210] after applying a band mask filter which extracted exclusively the diffuse intensities, see circles in the Fourier transforms. The shift between the APDs is emphasized by the inserted arrows.

these images display characteristic periodic changes which are shown in the orientation $[\bar{1}11]$ for different defocus value. Obviously, the cell of the ordered structure is doubled compared to the cell of the average structure. The contrast of the images correlates well in a defocus series with simulated images calculated on the basis of one of the ordered superstructure models A or B (see Fig. 5 and Table 1). The relationship between structure and contrast is shown for Scherzer defocus in Fig. 4, bottom. Due to the ordering of indium atoms in the superstructure model the contents of the marked regions in the projection of the structure are different from case (I), which leads to characteristic changes of the contrast in high-resolution images (see marks in Fig. 4). The good agreement between the contrast of experimental and simulated images can also be observed in all other examined zone axes, giving evidence for a correct description of the structure of the ordered crystals by the structure models A or B.

(III) Crystallites with short-range order displaying diffuse intensities surrounding the positions hkl with $l = 2n + 1$ in the FFTs are shown in Fig. 6 for zone axis $[\bar{1}11]$. The shape of the diffuse intensities in the FFTs is found to be the same as the observed one in the corresponding diffraction patterns (see Fig. 6, bottom left, and Fig. 1b, left). The intensity of the diffuse scattering in the FFTs shows large variations in different regions of the crystals indicating different degrees of order; see examples in Fig. 6. This corresponds to the significant contrast changes in the image indicating the presence of microdomains of an ordered structure. The images of crystals with microdomains are difficult to interpret because of the averaging between the different domains; however, the contrast of the individual ordered domains is equivalent to the one found for case (II). Information about the size of the domains and their relative orientations could be obtained by applying a Fourier filter which extracted the diffuse intensities for the inverse Fourier transformation. The resulting images (demonstrated in Fig. 7, for the zone axis $[\bar{1}11]$ and [210]) may show artifacts due to the filtering. Yet, they verify the presence of ordered microdomains. These figures display clearly that there are two types of microdomains which are shifted to each other by a well-defined translation. On closer examination of the images taking into account different orientations, e.g. [210], the shift vector corresponds to $\frac{1}{2}\vec{c}$ referring to the cell of the superstructure models.

All three cases (I)–(III) suggest the existence of a complex microstructure of domains. The essential feature in the real structure of $K_2In_{12}Se_{19}$ is the presence of domains with

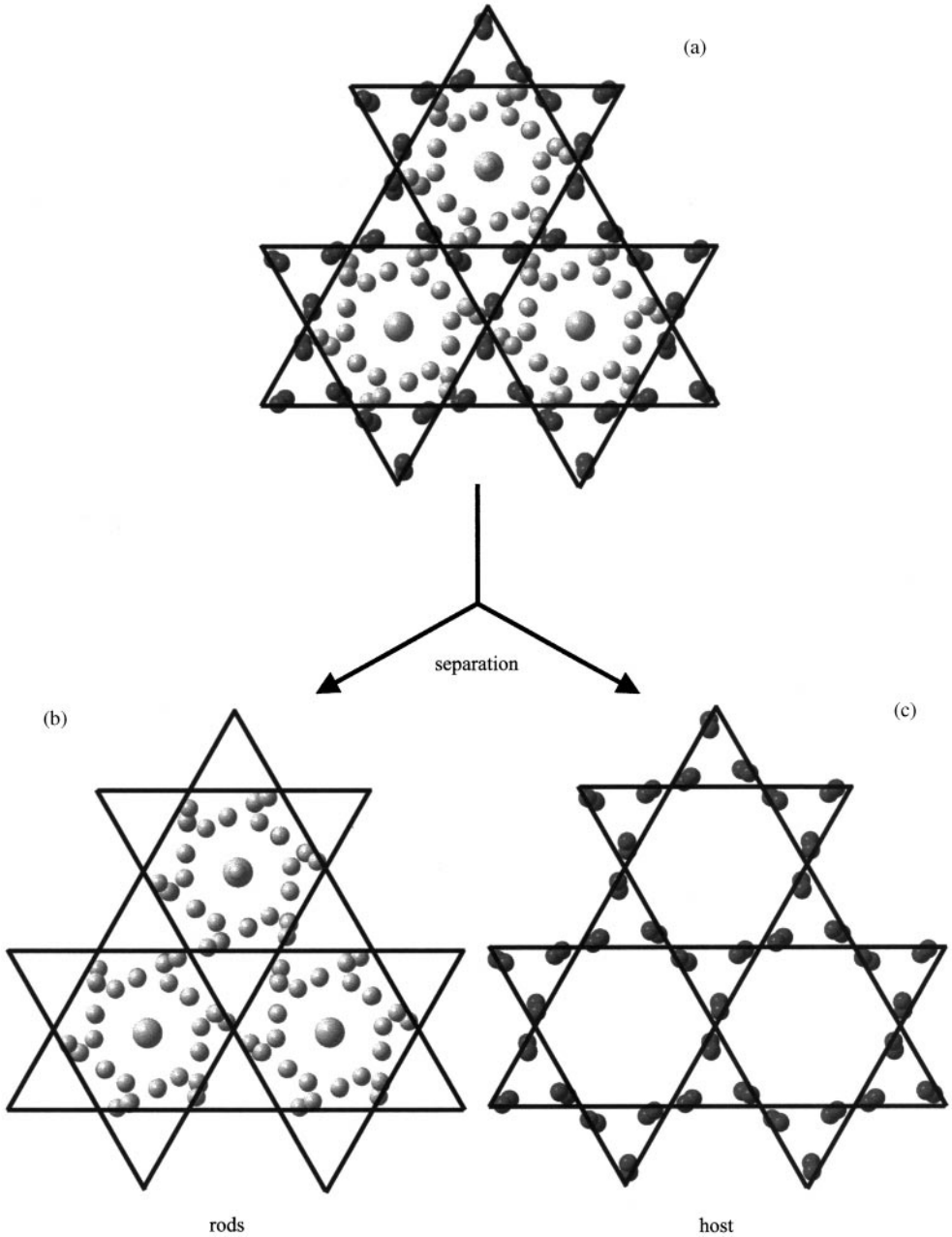

FIG. 8. Separation of the structure of $K_2In_{12}Se_{19}$ along a Kagomè net shown for the orientation [001]. The rods are built by the atoms displayed in light gray color (located in the hexagons of the superimposed Kagomè net, see (b)); the indium and selenium atoms of the frame placed in the triangles of the Kagomè net (see (a)) are shown in dark gray.

variable sizes, each consisting of one of the two possible superstructures described above. In case (I) a seemingly disordered structure with no short-range order results from superimposing unit cells of both superstructures on a very fine scale in the sense of a disordered intergrowth. It is important to emphasize that these crystallites are not formed from the unit cells of the average structure due to the discussed structural anomalies. In cases (II) the microdomains reach a size of several nanometers, and possibly complete crystallites consist of one domain only. Case (III) is the intermediate between cases (I) and (II). The domain structure of the crystals can be interpreted on the basis of ordered microdomains of both types of possible superstructures which are separated by APBs. The different antiphase domains (APDs) easily adjust to each other because of the existence of the pseudo-translation by $\frac{1}{2}\vec{c}$ which includes all atoms except In2a,b and In3a,b.

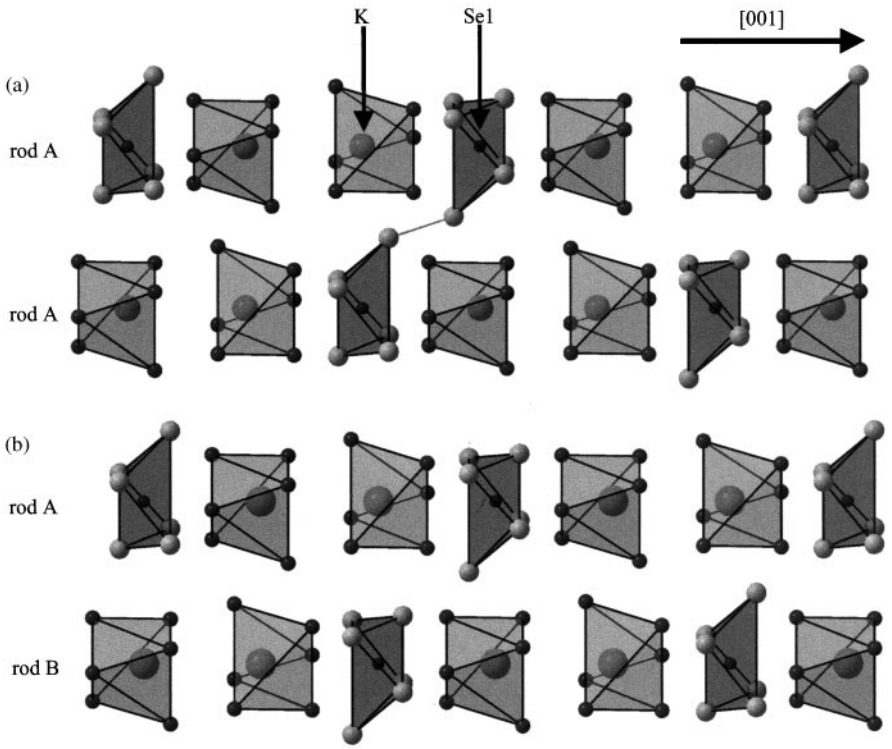

FIG. 9. Neighboring rods in the structure of $K_2In_{12}Se_{19}$. The coordination of the atoms Se1 (by In) and K1 and K2 (by Se) are displayed in polyhedral representation. (a) Neighboring rods in position A generate an unusually short distance d_{In-In} (indicated by the line); (b) one rod in position A and one rod in position B.

In conclusion the diffuse diffraction phenomena observed around *hkl* with $l = 2n + 1$ depend strongly on the domain size adopting different ranges of ordering between short- and long-range order.

Models of the Real Structure

For a better understanding of the observations obtained by electron diffraction and HREM it is necessary to find a description of the structure of $K_2In_{12}Se_{19}$ based on disorder of structural elements ordered in themselves.

The structure can be divided into two parts, a Kagomè-like partial structure ("host structure") of indium and selenium atoms and inserted rods parallel to [001] which contain those indium positions (In2, In3) which were found to be disordered in the average structure. The projection of the structure along [001] displays these features together with a superimposed Kagomè net (see Fig. 8). In this projection the atoms of the host structure are located inside the triangles while the rods are positioned within the hexagons of the Kagomè net. The two possible three-dimensional periodic superstructures possess the same host structure, and all atoms of this structure exhibit the pseudotranslation by the vector $\frac{1}{2}\vec{c}$. The essential difference between the superstructures lies in the two different positions of the otherwise identical rods (called A and B according to superstructure model A and B) shifted by the vector $\frac{1}{2}\vec{c}$ relative to each other. In the case of a crystal containing APDs these different positions of the rods coexist.

The interatomic distances of the indium atoms within a single rod and between two different rods are essential. The formation of the superstructures discussed results in an optimal value d_{In-In} (shortest distance, 3.949 Å) within a single rod. The distances between rods constitute a more complicated problem because of the possibility of a disorder of the rods in positions A and B. Two different combinations of the rods exist: rod A (B) neighboring rod A (B) and another one with rod A (B) neighboring rod B (A) (see Fig. 9). The last case is exclusively realized in domain crystals and leads to the formation of APB. A disordered crystal with both arrangements of the rods is characterized by $d_{In-In} = 3.528$ Å for combination AA (BB) and $d_{In-In} = 4.049$ Å for combination AB as shortest distances between indium atoms of different rods, respectively. An ordered crystal with only AA or BB arrangements shows $d_{In-In} = 3.528$ Å, i.e., electrostatically unfavorable contacts between the rods. Formation of APB in the case of a disordered crystal increases the interatomic distances between the indium atoms.

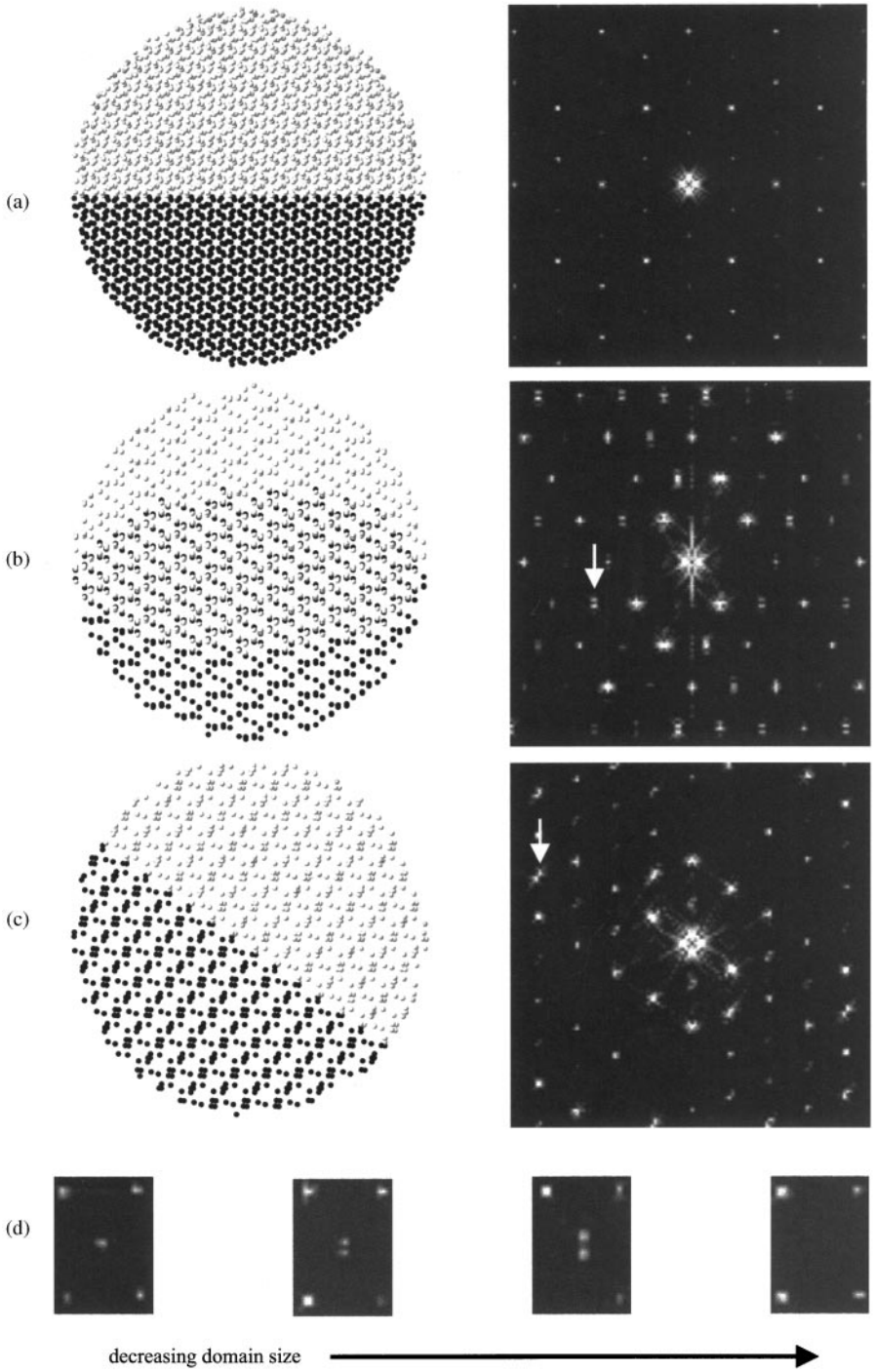

FIG. 10. Crude simulation of the diffuse scattering in different orientations. The displayed spheres of the structure have a diameter of 134 Å. (a) [001], (b) [$\bar{1}$11], (c) [100], examples of diffuse intensities are marked by an arrow. (d) Influence of the domain size on the shape of the diffuse scattering, orientation [$\bar{1}$11]. The distance between the double spots with diffuse intensity increases with decreasing domain size.

For topological reasons it is in principle not possible to reach the optimum configuration with rods in position A having exclusively neighbors of rods in position B and vice versa in an undistorted structure. This becomes immediately clear by looking at the best feasible configurations of the triangles (AAB and ABB). Even in these optimal cases neighboring rods in position A or rods in position B are present. This special peculiarity of the real structure of

$K_2In_{12}Se_{19}$ could be characterized by the concept of structural frustration (18). In conclusion the real structure of $K_2In_{12}Se_{19}$ is a compromise resulting in the formation of microdomains of an ordered structure, which are disordered.

Approximate Simulation of the Diffuse Scattering

In order to confirm the developed real structure model of $K_2In_{12}Se_{19}$ its diffuse scattering was simulated by Fourier transformation of images of the real structure. As a first approach only the indium atoms within the different rods are taken into account because the intensity of the diffuse scattering depends on the structural difference between rods of types A and B, i.e., on the differences in the positions of the indium atoms in the different rods. These simulations consist of two steps. (I) A three-dimensional but nonperiodic real structure model of ordered microdomains separated by APB must be constructed. Starting from the zone axis orientation [001] we created spheres that consist of ordered domains each containing one type of rod (A or B) only. As the diffuse intensities of the [001] pattern are located in the FOLZ the Fourier transform of this picture shows no diffuse scattering (see Fig. 10). (II) This three-dimensional structure model is then tilted to orientations that should exhibit diffuse scattering and the Fourier transforms are calculated. In this way we were able to qualitatively reproduce the diffuse scattering of several experimentally exam ined orientations, for instance [100] and [$\bar{1}$11] (see Figs. 10b, 10c and Figs. 1a, 1b).

The simulations are also very useful to show the influence of the domain size on the shape of the diffuse intensities, starting from one extreme case, the ordered crystal with sharp superstructure reflections in the FFT (Fig. 10d, left) and ending in the disordered crystal formed by superimposing the two possible ordered rods on a microscopic scale. The FFT shows exclusively sharp Bragg reflections corresponding to the average structure (Fig. 10d, right). The simulations in Fig. 10 indicate that for the intermediate cases an increasing distance between the diffuse intensity maxima occurs with decreasing size of the single domains. This leads to an increasing size of the internal diameter of the diffuse rings in FOLZ in the orientation [001] with decreasing size of the ordered domains.

Soon the domain structure of $K_2In_{12}Se_{19}$ will be analyzed by numerical Fourier transformation in order to get a full simulation of the reciprocal space including higher order Laue zones. The main goal of these simulations is to quantify the range of domain sizes and their distribution. Averaging over larger crystal volumes these two main features of the real structure determine the sharp profile and circular shape of the diffuse scattering. First simulations indicate that the range of domain sizes is very narrow. Thus the APBs of the domains should approximately be equispaced. A second important point is the orientation of the APB. In [001] they must be randomly orientated, thus being responsible for the circular character of the diffuse intensities in the FOLZ of this orientation. The results of the numerical Fourier transformation will be discussed in a separate publication.

ACKNOWLEDGMENTS

The authors thank Viola Duppel for practical electron microscopy work and assistance in designing the figures, M. Schlosser for the preparation of the samples, and Dr. C. Reiner and Prof. Dr. H. J. Deiseroth for helpful discussions.

REFERENCES

1. C. Reiner, Dissertation, Universität Siegen, 1999.
2. H. Jagodzinski and F. Frey, "International Tables for Crystallography," Vol. B. Kluwer Academic, Dordrecht, 1993.
3. F. Frey, *Z. Kristallogr.* **212,** 257 (1997).
4. M. Schlosser, C. Reiner, H. J. Deiseroth, and L. Kienle, *Eur. J. Inorg. Chem.* **9,** 2241 (2001).
5. A. I. Goldman, C. A. Guryan, C. A. Stephens, J. Parsey, Jr., J. M. Aeppli, H. S. Chen, and F. W. Gayle, *Phys. Rev. Lett.* **61,** 1962 (1988).
6. S. Esmaeilzadeh, J. Grins, and A.-K. Larsson, *J. Solid State Chem.* **145,** 37 (1999).
7. R. Miida, M. Tanaka, H. Arashi, and M. Ishigame, *J. Appl. Cryst.* **27,** 67 (1994).
8. S. Suzuki, M. Tanaka, and M. Ishigame, *J. Phys. C* **20,** 2963 (1987).
9. J. G. Allpress and H. J. Rossel, *J. Solid State Chem.* **15,** 68 (1975).
10. N. H. Andersen, K. Clausen, M. A. Hackett, W. Hayes, M. T. Hutchings, J. E. MacDonald, and R. Osborn, *Physica is B* **136**, 315 (1986).
11. R. B. Neder, F. Frey, and H. Schulz, *Acta Crystallogr. A* **46,** 799 (1990).
12. M. Schlosser, L. Kienle, C. Reiner, and H. J. Deiseroth, 10 Vortragstagung GdCh, 26, 29.9.2000, Münster.
13. P. A. Stadelman, *Ultramicroscopy* **21,** 131 (1987).
14. A. Redjaimia and J. P. Morniroli, *Ultramicroscopy* **53,** 305 (1994).
15. J. P. Morniroli and J. W. Steeds, *Ultramicroscopy* **45,** 219 (1992).
16. H. Bärnighausen, *Match* **9,** 139 (1980).
17. "International Tables for Crystallography," Vol. A. Kluwer Academic, Dordrecht, 1993.
18. U. Steinbrenner and A. Simon, *Z. Kristallogr.* **212,** 428 (1997).